Thermochimica Acta 562 (2013) 22–28

Contents lists available at SciVerse ScienceDirect

Thermochimica Acta

journal homepage: www.elsevier.com/locate/tca

Urease and α-chymotrypsin inhibitory activities of transition metal complexes of new Schiff base ligand: Kinetic and thermodynamic studies of the synthesized complexes using TG–DTA pyrolysis

Muhammad Ikram[a,*], Sadia Rehman[a,b], Muhammad Ali[c], Faridoon[b], Carola Schulzke[g], Robert J. Baker[d], Alexander J. Blake[e], Khan Malook[f], Henry Wong[e], Saeed-Ur-Rehman[b]

[a] Department of Chemistry, Sarhad University of Science and Information Technology, Peshawar, Pakistan
[b] Institute of Chemical Sciences, University of Peshawar, Pakistan
[c] Department of Biotechnology, Bacha Khan University Charsadda, Pakistan
[d] School of Chemistry, University of Dublin, Trinity College, Dublin 2, Ireland
[e] School of Chemistry, The University of Nottingham, Nottingham NG7 2RD, UK
[f] Centralized Resource Laboratory, University of Peshawar, Pakistan
[g] Institut für Biochemie, Ernst-Moritz-Arndt, Universität Greifswald, Felix-Hausdorff-Straße 4, 17487, Greifswald, Germany

ARTICLE INFO

Article history:
Received 26 December 2012
Received in revised form 14 March 2013
Accepted 18 March 2013
Available online 30 March 2013

Keywords:
Schiff base ligand
Coordination compounds
Urease and α-chymotrypsin inhibitory activities
Molecular modeling study
Thermo gravimetric analysis
Kinetic and thermodynamic study

ABSTRACT

The Schiff base 2-[(*E*)-(quinolin-3-ylimino)methyl]phenol (H-QMP) was crystallized in *Pc* space group and complexed with Ni(II) and Co(II) in $[M(QMP)_2]$ and Cu(II) and Zn(II) in $[M(QMP)(CH_3COO)]H_2O$ compositions. Elemental analyses, mass spectrometry, IR, UV–vis spectroscopy, conductance study and magnetic susceptibilities were used to characterize the complexes. The thermograms obtained in the range of 30–1000 °C were used for kinetic and thermodynamic calculations. The activation energies and order of pyrolysis were calculated using Horowitz–Metzger method. The calculated activation energies were subsequently used for the calculations of thermodynamic parameters including ΔS^*, ΔH^* and ΔG^*. It was found that the thermal stability and activation energy follow the order Cu(II) > Ni(II) > Co(II) > Zn(II) and $E^*_{Ni} > E^*_{Cu} > E^*_{Co} > E^*_{Zn}$, respectively. All the compounds were also studied for their urease and α-chymotrypsin inhibition, showing medium to moderate activities for both the enzymes except nickel complex. Nickel complex shows $IC_{50} = 9.9 \pm 0.124\ \mu M \pm SEM$, and the activity was rationalized by carrying out molecular modeling studies.

1. Introduction

Nickel containing enzyme, urease, is involved in the rapid hydrolysis of urea to form ammonia and carbamate. The carbamate consequently multiplies again to produce another molecule of ammonia. This enzymatic behavior can be seen in various organisms like algae, fungi, bacteria and even human beings which causes an abrupt elevation in the blood pH with side effects like cell death, kidney failure, severe ulcer, urolithiasis, pyelnephritis, and hepatic encephalopathy, hepatic coma and urinary catheter encrustation [1–14]. The structure of this unique enzyme had been studied in detail by Musiani et al. using DOCK for calculating stability based on energies of the enzyme. The structure of the enzyme shows the terminal —OH groups which are directly involved in covalent bond formation when the enzyme interacts with tested molecules or it form hydrogen bonds with the interacting molecules as shown in Scheme 1 [15].

Due to the diverse functions of this enzyme, its inhibition by potent and specific compounds could provide an invaluable addition for treatment of infections, and secondary complexes such as pus formation and ulcer caused by urease-producing bacteria. Such kind of inhibitors can inhibit the enzymatic actions by attaching either to the —OH groups of the enzymes or by just only hydrogen bond formation. Metal complexes which have the ability to interact with anionic centers like —OH groups can effectively inhibit urease. Therefore we synthesized the metal complexes of salicyldehyde derived Schiff base ligand. Schiff base ligand was prepared by the condensation of salicyldehyde with 3-aminoquinoline. Schiff base derivatives of salicylaldehydes were treated as monoanionic ligands and were employed as bidentate ligands coordinating through N/O sites of attachments. We have communicated about the structural features of the compounds where H-QMP is acting as ligand can be seen in our already reported work [16]. In the recent years, there has been considerable interest in the chemistry of transition metal complexes of Schiff bases which offer

* Corresponding author. Tel.: +92 334 9321879.
E-mail address: ikram.chemistry@suit.edu.pk (M. Ikram).

0040-6031/$ – see front matter © 2013 Elsevier B.V. All rights reserved.
http://dx.doi.org/10.1016/j.tca.2013.03.026

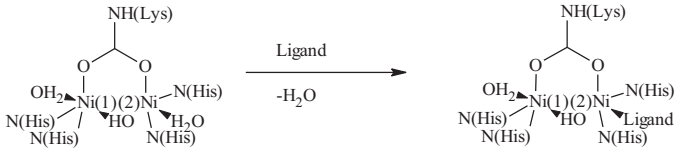

Scheme 1. Mechanism of interaction of inhibitors with urease.

opportunities for inducing substrate chirality and reorientations in geometry around the metal center thereby tuning electronic configuration of the metal center [17–21]. Schiff bases have been also found to enhance the solubility and stability of either homogeneous or heterogeneous catalysts [22–27]. Herein we report the synthesis and crystal structure of a monoanionic ligand. Apart from it the same metal complexes were also tested for their α-chymotrypsin inhibitory activities. α-Chymotrypsin (EC 3.4.21.1), a protease, which is secreted from pancreas, catalyzes the breakdown of polypeptide and proteins. If the precursor of chymotrypsin, the chymotrypsinogens is cleaved to form active enzyme before the target side, then it digest the tissues inside body such as in cases of pancreatitis [28,29]. α-Chymotrypsin has been found to be involved in clearance of ulcer, digesting damaged tissue and debris in the infected site [20–29]. Therefore a drug which is active against urease activities and inactive against α-chymotrypsin may help in healing the peptic ulcers, etc. very efficiently. Here we are reporting the structural details of H-QMP along with thermal degradation studies in continuation to our previous work reported [30]. The thermal data was used for the calculation of kinetic and thermodynamic parameters. All the compounds were also studied for their urease and α-chymotrypsin inhibitory activities. Nickel complex was found to be much more active than the standard drug.

2. Experimental

The detailed synthesis and characterization can be found in our earlier report [16]. The codes assigned to the compounds follow the trend given below:

2-[(*E*)-(quinolin-3-ylimino)methyl]phenol **(H-QMP)**

Bis(2-[(*E*)-(quinolin-3-ylimino)methyl]phenolato)nickel(II) **(1)**

Bis(2-[(*E*)-(quinolin-3-ylimino)methyl]phenolato)cobalt(II) **(2)**

2-[(*E*)-(quinolin-3-ylimino)methyl]
phenolatoacetatoaquocopper(II) **(3)**

2-[(*E*)-(quinolin-3-ylimino)methyl]
phenolatoacetatoaquozinc(II) **(4)**.

2.1. Urease inhibition assay

Exact 25 μL of enzyme (jack bean urease) solution and 5 μL of test compounds (0.5 mM concentration) were incubated with 55 μL of buffers containing 100 mM urea for 15 min at 30 °C in each well of 96-well plates. Ammonia production was measured as a urease activity by indophenol method. Final volumes were maintained as 200 μL by adding 45 μL phenol reagent (1%, w/v phenol and 0.005%, w/v sodium nitroprussside), and 70 μL of alkali reagent (0.5%, w/v NaOH and 0.1% active chloride NaOCl) to each well. Using a microplate reader (Molecular Devices, CA, USA), the increase in absorbance was measured at 630 nm after 50 min at pH 6.8 [27,28].

2.2. α-Chymotrypsin inhibition assay

This was performed in 50 mM Tris–HCl buffer pH 7.6 with 10 mM $CaCl_2$ according to Cannell et al. [29] with the slight modification. α-Chymotrypsin (12 units/mL prepared in buffer) with the various concentrations of test compound (prepared in DMSO) was incubated at 30 °C for 25 min. The reaction was started by adding *N*-succinyl-L-phenylalanine-*p*-nitroanilide (prepared in buffer) at final concentration of 0.4 mM. The change in absorbance was continuously monitored at 410 nm.

2.3. Crystal structure determination

Suitable single crystal for X-ray structural analyses of **H-QMP** were mounted on a glass fiber, and the respective data were collected on Oxford diffractometer (graphite-monochromated Mo Kα radiation, λ = 0.71073 Å) at 298 K. The structures were solved with the olex2.solve [31] refined against all data by full-matrix least-squares methods on F^2 (SHELXL-97) [32]. All non-hydrogen-atoms were refined with anisotropic displacement parameters. The hydrogen atoms were refined isotropically on calculated positions using a riding model with their U_{iso} values constrained to 1.5 U_{eq} of their pivot atoms for terminal sp^3 carbon atoms and 1.2 times for all other carbon atoms. Crystallographic details are given in the supplementary information file. CCDC-885677 (H-QMP) data can be obtained free of charge from the Cambridge Crystallographic Data Center via www.ccdc.cam.ac.uk/data_request/cif.

2.4. Docking

The molecular docking of the inhibitor with the 3D crystal structure of urease from *Bacillus pasteurii* downloaded from protein data bank (PDB code: 4UBP) was performed with AutoDock Vina program [33]. Autodock Tool was used to remove water molecules and non-standard protein residues from the urease enzyme. The polar hydrogens were added and charges were assigned with Gasteiger method. The active sites were defined and the structure of the enzyme as receptor in the required pdbqt format was saved. The docking site on the receptor macromolecule was defined by fixing the grid box with the dimensions 40 × 40 × 40 Å with grid spacing of 0.375 Å centered on Ni841 in the active site of the protein.

3. TG–DTA analysis

The TG–DTA analyses were carried out using TG/DTA Diamond model by Perkin Elmer at heating rate 10 °C min^{-1} in temperature range 30–1000 °C under static air. Specific mass of samples were contained in ceramic pans crucibles adjusted on platform support giving a proportional signal to recorder, observed by computer interface and the results were plotted in the form of mass loss of sample vs. temperature for TG and microvolts vs. temperature for DTA. All the results were referenced to thermal decomposition of alumina. The activation energies of all the samples were calculated using Horowitz–Metzger method [34]. It was found that linear plots can be obtained while $\ln \ln(Wo - W_t^f)/(W - W_t^f)$ {where *Wo* = initial mass taken, *W* = weight remaining at a given temperature, W_t^f = final weight} were plotted against Θ {where $\Theta = T_c - T_s$}. The slope of the straight line was used to calculate the activation energy through the expression (1):

$$\text{Slope} = \frac{E^*}{RT_s^2} \quad (1)$$

Order of decomposition was calculated from the relationship between reaction order and concentration at maximum slope [34]. Thermodynamic parameters of activation were evaluated by using the following expressions (2)–(4), respectively [35]:

$$\Delta S^* = 2.303 \ \log\left[\frac{Ah}{k_B T_s}\right] R \quad (2)$$

$$\Delta H^* = \Delta E^* - RT \quad (3)$$

$$\Delta G^* = \Delta H^* - T\Delta S^* \quad (4)$$

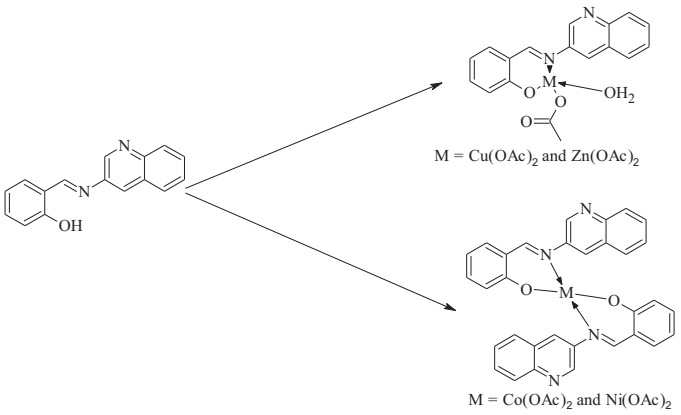

Scheme 2. Metal complexation by H-QMP.

4. Results and discussion

The ligand H-QMP was synthesized by condensing salicyaldehyde with 3-aminquinoline to yield the phenolic Schiff base ligand [16]. The ligand H-QMP was reacted with the divalent metal ions of Ni, Co, Cu and Zn as shown in Scheme 2. The synthetic methods and the structural features were discussed in our earlier report [16].

4.1. Crystal structure of H-QMP

The ligand H-QMP co-crystallizes out from the concentrated THF solution in *Pc* space group. The cocrystallization was handled with free variables but the atoms on identical positions were refined jointly (i.e. same position, same displacement factors but complementing occupation). About 70% is the wanted molecule and 30% of the bisquinoline is present in the crystals obtained. There is a lot of electron density between Schiff base N and phenolic O which could be a partial carbon (about 35% according to an initial test) and oxygen is only about 65% oxygen and about 35% nitrogen and that affects the hydrogen attached to the oxygen as well, same for N(3) (mixture of carbon and nitrogen). C(17) actually is not present in the H-QMP core structure but due to accumulation of electron density, it looks like a cyclic ring is produced.

The ORTEP plot (Fig. 1) of H-QMP shows that the plane C(10)—C(11)—C(12)—C(13)—C(14)—C(15)—C(16) is separated by 1.34° from the plane produced by C(1)—C(2)—C(3)—C(4)—C(5)—C(6)—C(7)—C(8)—C(9)—N(1) showing perfect coplanarity between the aromatic rings. Whereas the plane of C(1)—C(2)—C(3)—C(4)—C(5)—C(6)—C(7)—C(8)—C(9)—N(1) is separated by 8.16° from the plane produced by N(3)—C(7)—C(2)N showing that the molecule is not acting entirely as bisquinoline, rather mixture of our synthesized Schiff base ligand and the co-crystalized bisquinoline. The same behavior may be observed by taking the planes C(10)—C(11)—C(12)—C(13)—C(14)—C(15)—C(16) and N(3)—C(7)—C(2)N, being separated by 9.29°. The torsion in the C(16)—N(3)—O(1)—N(2)—C—(2N) is greater by −6.58° than the torsion in C(14)—C(15)—C(16)—C(11) revealing the false nature of the aromatic ring produced by the atoms N(3)—O(1)—C(17)—N(2)—C(2N). The intramolecular hydrogen bonding between the imine nitrogen and the hydrogen of hydroxyl group results in the formation of non-planar six membered distorted rings. The bond length for this intra molecular hydrogen bond was found to be 1.78 Å comparable to the O—H···N bond length in $C_{16}H_{17}NO_2$ [36]. A unique cress cross type arrangement can be observed in the crystal lattice. This unique arrangements is due to the hydrogen bonding explicitly connecting aminoquinoline nitrogen with H(10) (2.471 Å). The —CH=N bond distance is 1.332 Å which was found to be longer than the normal bond length of imine linkage as found in (*R*)-4-methoxy-2-[(1-phenylethyl)iminomethyl]phenol (1.283 Å) [37]. This may be due to presence of electron deficient aminoquinoline ring. The crystal data is reported in Table 1 (Fig. 2).

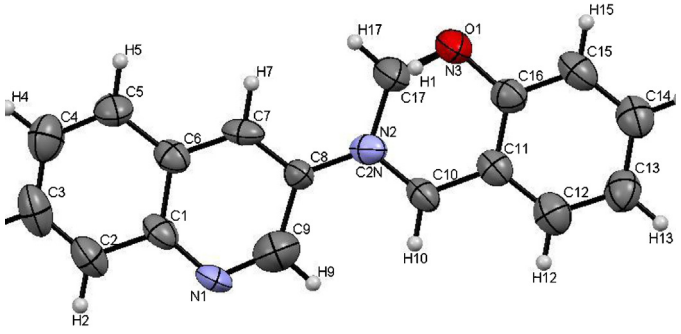

Fig. 1. Molecular structure of H-QMP. H atoms are shown.

Table 1
Crystal data and structure refinement for H-QMP.

Identification code	H-QMP
Empirical formula	$C_{17}H_{13}N_2O$
Formula weight	248.27
Temperature (K)	293
Crystal system	Monoclinic
Space group	P_1c_1
a (Å)	8.9245(11)
b (Å)	6.3535(7)
c (Å)	12.318(2)
α (°)	90.0
β (°)	116.288(11)
γ (°)	90.0
Volume (Å^3)	626.22(16)
Z	1
2*Θ* range for data collection	6.42–56.16°
Index ranges	$-11 \le h \le 11, 0 \le k \le 8, -15 \le l \le 15$
Reflections collected	5061
Independent reflections	4097[*R*(int) = 0.0297]
Data/restraints/parameters	4097/0/344
Goodness-of-fit on F^2	1.409528
Final *R* indexes [$I \ge 2\sigma(I)$]	R_1 = 0.092214
Final *R* indexes [all data]	R_1 = 0.142673
Largest difference peak/hole/e (Å^{-3})	1.039395/−0.369261

4.2. Urease and α-chymotrypsin activities

Compounds can be classified into two categories based on their urease inhibitory activities (1) organic compounds which include acetohydroxamic acid, humic acid, etc. and (2) heavy metal ions which include Cu^{2+}, Zn^{2+}, Pd^{2+}, and Cd^{2+}. Rarely metal complexes were tested for the inhibition of urease and α-chymotrypsin. Table 2 enlists the inhibition of urease and α-chymotrypsin by all the tested metal complexes. The results reveal that nickel

Table 2
Inhibitory activities of 0.05 mM against α-chymotrypsin and urease enzymes.

Compound	IC_{50} for α-chymotrypsin (μM) ± SEM	IC_{50} for urease (μM) ± SEM
H-QMP	–	–
1	–	9.9 ± 0.124
2	–	–
3	–	–
4	–	–
Thiourea[a]	–	21 ± 0.011
Chymostatin[b]	5.71 ± 0.13	–

[a] Standard inhibitor of urease.
[b] Standard inhibitor of α-chymotrypsin.

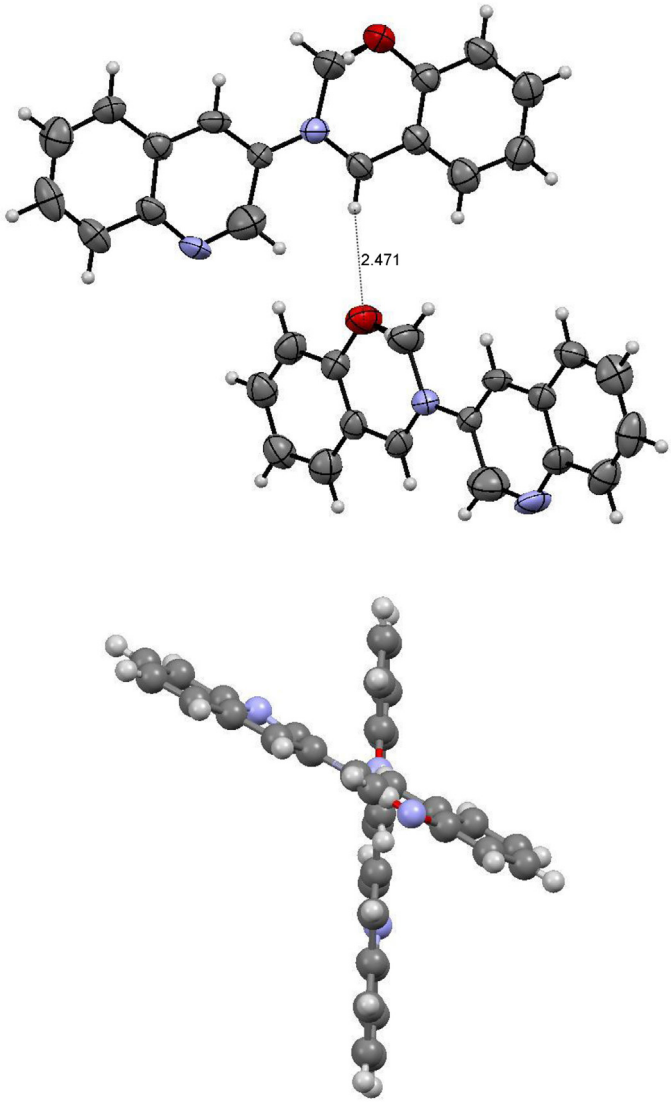

Fig. 2. Crystal packing pattern in H-QMP crystal lattice.

complexes are much more active for urease inhibition than any other metal complex. At the same time it is observed that complex **1** is showing much lower activity against α-chymotrypsin. Therefore nickel centered metal complexes of the H-QMP ligand can help in designing selective drugs. This selectivity of the nickel containing compound to inhibit urease may be attributed to chelation by H-QMP. Other metal complexes with the same ligand were not found to be so much active against any of the tested enzyme. Cobalt centered complex of the ligand H-QMP is also showing activity which ranges from moderate inhibition of α-chymotrypsin to the high activity for urease. By comparing **1** and **2** it can be concluded that nickel is selective inhibitor for urease. Previous study on the urease activities have shown that metal complexes of Sn(IV), Cu(II), Bi(III), Cu(II) and Cd(II) were found to be active [25]. Here we are extending the inhibition of urease by nickel (II) complex of H-QMP. The inhibition of urease by **1** may be explained by the possible interaction of the metal ion with —OH bridge group in the enzyme. This may either lead to Ni—Ni weak interaction as well which will affect the activity of enzyme. Therefore it can be presumed that metal ions which are involved in the interaction with the bridging —OH group will be active in the inhibition process [25]. Apart from it **2** is also showing inhibition of the urease enzyme upto some extent but unlike **1** is not selective by inhibiting chymotrypsin as

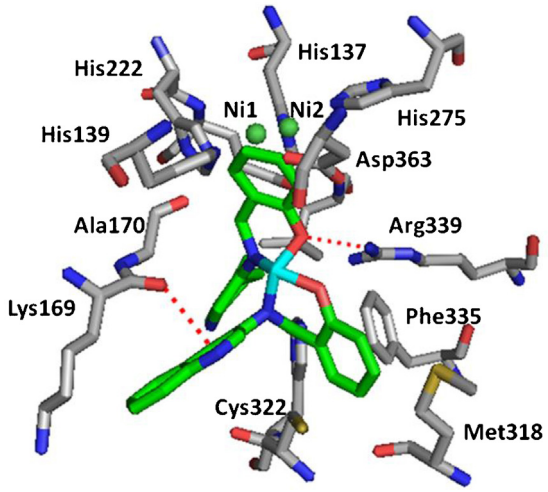

Fig. 3. The binding mode of complex **1** in the active site of urease enzyme from *Bacillus pasteurii*. Atom colors: blue-nitrogen, red-oxygen, green-carbon (inhibitor), gray-carbon (enzyme), yellow-sulphur and cyan-Ni ion (inhibitor). Red dotted lines show hydrogen bonds. (For interpretation of the references to color in the text, the reader is referred to the web version of the article.)

well. Complexes **3** and **4** are not showing any convincing inhibition for both the tested enzymes. Recently in our previous communication about the inhibition of urease by copper complexes has also been reported. Copper square planar complexes were found much more active than the Schiff base ligands [30]. Therefore it can be concluded that square planar complexes are effective in inhibition process as compared to tetrahedral **3** and **4**.

4.3. Molecular docking study

In order to rationalize the structure-activity relationship (SAR), the molecular docking of nickel complex **1** in the active sites of urease enzyme from *Bacillus pasteurii* (PDB code: 4UBP) was performed. The binding mode of **1** with urease enzyme is depicted in Fig. 3 and the enzyme surface model is shown in Fig. 4. The result revealed that the complex molecule was well filled in the active pocket of urease enzyme. The chelating phenolic oxygen atom of the complex formed hydrogen bond with the amino group of Arg339 with the hydrogen-bonding distance of 3.5 Å ($O_{complex}\cdots H—N_{Arg339}$). The nitrogen atom of quinoline of the ligand has the polar interaction with the hydroxyl group of Lys169 of the urease enzyme. The hydrogen-bonding distance is 3.3 Å ($N_{complex}\cdots H—O_{Lys}$). However, the complex also has hydrophobic

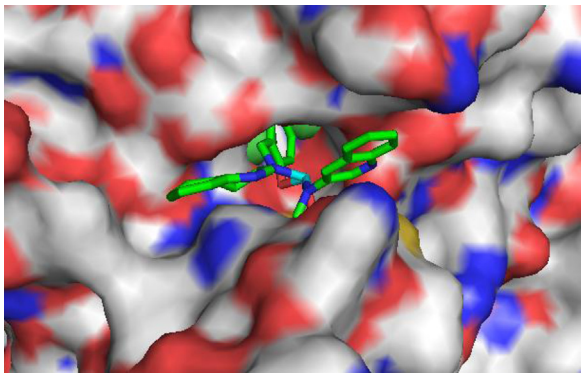

Fig. 4. Binding mode of **1** with urease from *Bacillus pasteurii*. The surface show the enzyme while the inhibitor is shown in sticks model. Colors of atoms: blue-nitrogen, red-oxygen, green-carbon and cyan-nickel. (For interpretation of the references to color in the text, the reader is referred to the web version of the article.)

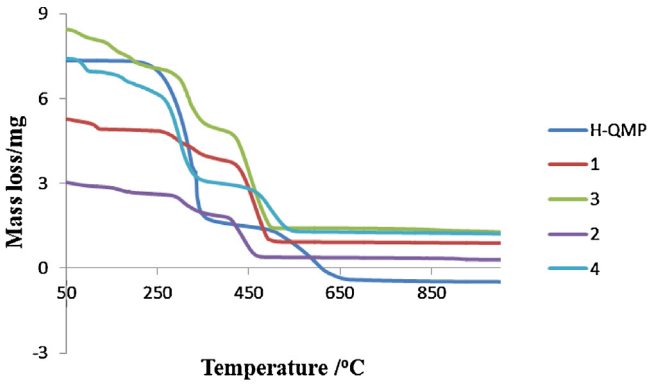

Fig. 5. Thermogravimetric plots of H-QMP and its metal complexes.

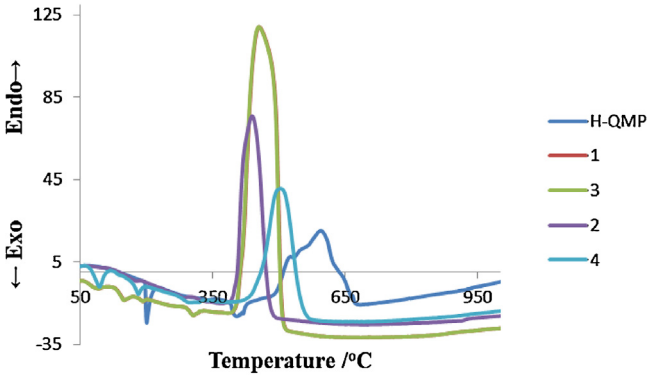

Fig. 6. Differential thermogravimetric curves for H-QMP and its metal complexes.

$$C_{16}H_{12}N_2O \rightarrow C_2H_2 + C_7H_5N + C_6H_5^{\bullet} + 1/2NO + 1/2CO$$

Scheme 3. Thermal degradation of H-QMP.

interactions with His324 and Cys322. The inhibitory activity of complex **1** against urease enzyme may be due to the two mentioned hydrogen bonding and hydrophobic interactions with enzyme in active pocket of urease enzyme.

4.4. Thermodynamics and thermal studies

Thermal pyrolysis of H-QMP ligand and its metal complexes were evaluated in the range of 30–1000 °C in static air. The TG and DTA curves are shown in Figs. 5 and 6, respectively. The complexes exhibited endothermic peaks corresponding to melting points and transition temperatures. Table 3 represents DTA and TG data for Schiff base ligand and its transition metal complexes. The TG curve for H-QMP shows that the compound is stable up to 200 °C and then follow the degradation process. The temperature at which a compound starts its decomposition is represented by T_d in Table 3. T_d for **1, 2, 3** and **4** are 240, 190, 310 and 180 °C respectively.

By looking into Table 3, it is apparent that the ligand exhibit five DTA peaks marking the five products of pyrolysis. The very large negative value for entropy, shown in Table 4, explains the stable nature of the ligand, also confirmed by high activation energy value. H-QMP follows single degradation step (shown in Scheme 3), producing the benzene free radical, quinolone, nitric oxide, carbon monoxide and acetylene, without any residue left at the end of process. The degradation process completes at 610 °C.

Both **1** and **2** are nickel and cobalt complexes of the H-QMP ligand having identical crystal structures, follow the same trend in degradation phenomenon. Both the complexes bear ethanol and methanol molecules in their crystal lattice respectively, which are

$$C_{32}H_{22}N_4NiO_2 \rightarrow C_2H_5OH \text{ in crystal lattice} + C_{32}H_{22}N_4NiO_2 \quad \text{I Stage}$$

$$C_{32}H_{22}N_4NiO_2 \rightarrow C_{30}H_{20}N_2NiO_2 + 2HCN \quad \text{II Stage}$$

$$C_{30}H_{20}N_2NiO_2 \rightarrow C_{18}H_{12}N_2 + C_{10}H + 2CO + NiO(\text{Residue}) \quad \text{III Stage}$$

Scheme 4. Thermal degradation of **1**.

$$C_{32}H_{22}CoN_4O_2 \rightarrow CH_3OH \text{ in crystal lattice} + C_{32}H_{22}CoN_4O_2 \quad \text{I Stage}$$

$$C_{32}H_{22}CoN_4O_2 \rightarrow C_{30}H_{20}CoN_2O_2 + 2HCN \quad \text{II Stage}$$

$$C_{30}H_{20}CoN_2O_2 \rightarrow C_{18}H_{14}N_2 + C_{10}H + 2CO + CoO(\text{Residue}) \quad \text{III Stage}$$

Scheme 5. Thermal degradation of **2**.

$$C_{18}H_{16}CuN_2O_4 \rightarrow H_2O + HOCN + C_{17}H_{13}CuNO_2 \quad \text{I Stage}$$

$$C_{17}H_{13}CuNO_2 \rightarrow 2CO_2 + C_{15}H_{13}CuNO \quad \text{II Stage}$$

$$C_{15}H_{13}CuNO \rightarrow C_9H_7N + C_6H_6O + Cu\ (\text{Residue}) \quad \text{III Stage}$$

Scheme 6. Thermal degradation of **3**.

evolved first when the sample is heated. In the second step hydrogen cyanide moiety is produced with two DTA peaks for **1** and one for **2**. In the third step both compounds exhibit identical behavior and produced two moles of quinolone in the form of free radicals and two moles of phenolate free radicals. The quinolone free radical moiety combined with each other to produce the stable bisquinoline species. Similarly the two phenolate free radicals might fuse together to produce naphthalene and two moles of carbon monoxide gas. The two endothermic DTA peaks for this fragmentation substantiate the results of TG data. In the last step both the compounds produces their corresponding oxides which are stable up to 1000 °C, the temperature to which compounds were heated. The negative entropy values for both the compounds differ only by $\Delta S^* = 15\,J\,mol^{-1}\,K^{-1}$. **1** follow 3/2 order of pyrolysis whereas **2** show 2nd order reaction process. By comparing the activation free energies for both the complexes, it is apparent that H-QMP produces more stable complex with nickel than cobalt. This is further evidenced by the values for enthalpy change and activation energy terms. The degradative routes for both **1** and **2** are shown below in Schemes 4 and 5, respectively.

For **3**, the thermal degradation starts at 140 °C and ends at 210 °C. The initial products are coordinated water and the isocyanic acid, an intermediate for cyanoric acid. In the second stage of degradation, started at about 230 °C, two moles of carbon dioxide is produced. In the third step ranging from 390 °C to 520 °C, the ligand based degradation occur, producing quinolone and phenol. Copper metal remain as residue as shown in Scheme 6. DTA peaks are consistent with the degradative products produced. There are three DTA peaks for first stage of pyrolysis, one for second and one for third. All the DTA peaks are negative except for the third stage which is +120. The entropy value for 3 is $-262.74\,J\,mol^{-1}\,K^{-1}$ indicating that the degradation reactions are slower than the normal reactions. The low activation energy value for **3** may be attributed to less stable complexes of the H-QMP ligand. The high value of activation free energy shows that the degradation process is endergonic with almost zero enthalpy change. The degradation is following the 5th order reaction process.

At about 100 °C, thermal degradation process of **4** was started, releasing 0.5 mole of water and the same amount of nitric oxide.

Table 3
Thermoanalytical results of H-QMP and its complexes.

Compound	TG temperature range (°C)	Decomposition temperature (°C)	Stage	Mass loss		DTA	Moiety evolved
				% calculated	% found		
H-QMP	30–610	200	I	101.4	100	(−)26, (−)18, (−)26.5, (+)0.30, (+)10.78	1/2NO, 1/2CO, C_2H_2, C_7H_5N, $C_6H_5^{\bullet}$
1	30–140	240	I	7.6	8.2	(−)10	C_2H_5OH (in crystal lattice)
	140–320		II	9.3	8.0	(−)13, (−)15	2HCN
	320–400		III	77.0	79.8	(−)12, (+)118	$C_{18}H_{12}N_2$, $C_{10}H_8O$, 2CO
	>400		Res	13.3	13.1	–	NiO
2	30–120	190	I	5.5	5.5	(+)2	CH_3OH
	120–300		II	9.8	9.7	(−)2	2HCN
	300–400		III	67	71.5	(−)9, (+)81.5	$C_{18}H_{12}N_2$, $C_{10}H_8O$, 2CO
	>400		Res	12.8	12.9	–	CoO
3	30–210	310	I	16.0	16.7	(−)0 .5, (−)5.6, (−)9.3	H_2O, HOCN
	210–390		II	22.7	23.4	(−)19 .0	$2CO_2$
	390–520		III	56.3	49.2	(+)120	C_6H_6O, C_9H_7N
	>520		Res	16.2	15.3	–	Cu
4	30–100	180	I	5.6	6.0	(+)2, (−)6	$1/2H_2O$, 1/2NO
	100–370		II	57.2	55.3	(−)10, (−)9	$C_9H_6N^{\bullet}$, $C_6H_5O^{\bullet}$
	370–560		III	26.3	25	(+)46	2CO, CO_2, $2H_2$
	>560		Res	16.0	15.0	–	ZnO

Table 4
Kinetic and thermodynamic parameters of H-QMP and its metal complexes.

Compound	Ts (K)	E^* (kJ/mol)	ΔH^* (kJ/mol)	ΔG^* (kJ/mol)	ΔS^*, (J mol^{-1} K^{-1})	Order of reaction, n
H-QMP	608.7	61.01	62.76	190.96	−210.62	1
1	727	51.85	54.05	246.85	−265.21	3/2
2	697	11.30	13.38	187.82	−250.26	2
3	588.1	13.79	15.97	170.45	−262.74	5
4	562	10.50	12.46	145.17	−236.15	5

The second stage completes at 370 °C, quinoline and phenol in the form of free radicals are released. Two moles of carbon monoxide and hydrogen gas, and one mole of carbon dioxide are produced leaving zinc oxide residue. Five DTA peaks are observed during the complete degradation process. In the first stage one endothermic as well as one exothermic peak is observed. Both the peaks are exothermic in the second stage, whereas in the third step endothermic peak can be seen. Fifth order kinetics is followed during the degradation process of **4**. −236.15 J mol^{-1} K^{-1} represents entropy of the process. The change in Gibb's free energy term is low with low enthalpy value, representing exogonic process. This is further supported by the low activation energy value. The degradation route of **4** can be seen in Scheme 7.

From the T_d values of all complexes it can be established that copper(II) complexes are stable. The order of stability varies in the order Cu(II) > Ni(II) > Co(II) > Zn(II) which follow the Irving William series of stabilities. From the activation energies the order of decreasing activation energy is $E^*_{Ni} > E^*_{Cu} > E^*_{Co} > E^*_{Zn}$.

$$C_{18}H_{16}N_2O_4Zn \rightarrow 1/2H_2O + 1/2NO + C_{18}H_{15}NO_2Zn \quad \text{I Stage}$$

$$C_{18}H_{15}NO_2Zn \rightarrow C_9H_6N^{\bullet} + C_6H_5O^{\bullet} + C_3H_4O_2Zn \quad \text{II Stage}$$

$$C_3H_4O_2Zn + O_2 \rightarrow 2CO + CO_2 + 2H_2 + ZnO\ (\text{Residue}) \quad \text{III Stage}$$

Scheme 7. Thermal degradation of **4**.

5. Conclusion

Novel nickel based urease inhibitor has been reported here which is found to be selectively involved in the urease inhibition with low inhibition of the chymotrypsin. Therefore a new metal based therapeutic agent can be developed for the treatment of various diseases like ulcers, kidney related diseases, coma, etc. Complex **1** was the most active inhibitor of urease with $IC_{50} = 9.9 \pm 0.124$ μM, comparable to the most potent urease inhibitors reported.

Molecular docking was used to examine the likely binding orientation of **1** in the active site of urease enzyme from *Bacillus pasteurii*. Cobalt, copper and zinc centered metal complexes were found inactive against both urease and chymotrypsin enzymes.

All the metal complexes show three step decomposition process whereas the corresponding ligand show a single step decomposition. Activation energies and order of the decomposition processes were investigated by Horrowitz method and the thermodynamic parameters were calculated by using the corresponding equations. The high thermal stability is shown by **3** or copper complex of the H-QMP ligand and it was concluded that the order of stability is Cu(II) > Ni(II) > Co(II) > Zn(II). Therefore it can be revealed that H-QMP may lead to greater stability in case of distorted tetrahedral geometry. This order is also consistent with Irving William series. From the activation energies it was found that the order of decreasing activation energies for the metal complexes is $E^*_{Ni} > E^*_{Cu} > E^*_{Co} > E^*_{Zn}$ whereas H-QMP displayed higher activation energy than either of its complexes. Except for **3** all the metal complexes decomposed to produce the corresponding oxides as residues, for **3** the residue was found to be copper metal.

Acknowledgment

The authors Muhammad Ikram and Sadia Rehman gratefully acknowledge the Higher Education Commission (HEC) Pakistan for providing financial assistance.

Appendix A. Supplementary data

Supplementary data associated with this article can be found, in the online version, at http://dx.doi.org/10.1016/j.tca.2013.03.026.

References

[1] P.A. Karplus, M.A. Pearson, R.P. Hausinger, 70 years of crystalline urease: what have we learned? Acc. Chem. Res. 30 (1997) 330–337.
[2] Z. Amtul, Atta-ur-Rahman, R.A. Siddiqui, M.I. Choudhary, Chemistry mechanism of urease inhibition, Curr. Med. Chem. 9 (2002) 1323–1348.
[3] W. Zaborska, M. Kot, K. Superata, Evaluation of the inhibition mechanism, J. Enzym. Inhib. Med. Chem. 17 (2002) 247–253.
[4] H.-Q. Li, Z.-P. Xiao, Y.-L. Luo, T. Yan, P.-C. Lv, H.-L. Zhu, Amines and oximes derived from deoxybenzoins as Helicobacter pylori urease inhibitors, Eur. J. Med. Chem. 44 (2009) 2246–2251.
[5] W.-J. Mao, P.-C. Lv, L. Shi, H.-Q. Li, H.-L. Zhu, Synthesis, molecular docking and biological evaluation of metronidazole derivatives as potent Helicobacter pylori urease inhibitors, Bioorg. Med. Chem. 17 (2009) 7531–7536.
[6] Z.-P. Xiao, D.-H. Shi, H.-Q. Li, L.-N. Zhang, C. Xu, H.-L. Zhu, Polyphenols based on isoflavones as inhibitors of Helicobacter pylori urease, Bioorg. Med. Chem. 15 (2007) 3703–3710.
[7] W. Zaborska, B. Krajewska, Z. Olech, Heavy metal ions inhibition of jack bean urease: potential for rapid contaminant probing, J. Enzym. Inhib. Med. Chem. 19 (2004) 65–69.
[8] W. Zaborska, B. Krajewska, M. Leszko, Z. Olech, Inhibition of urease by Ni^{2+} ions. Analysis of reaction progress curves, J. Mol. Catal. B: Enzym. 13 (2001) 103–108.
[9] M.I. Khan, M.K. Baloch, M. Ashfaq, Spectral analysis and invitro cytotoxicity profiles of novel organotin(IV) esters of 2-maleimidopropanoic acid, J. Enzym. Inhib. Med. Chem. 22 (2007) 343–350.
[10] R. Ara, U. Ashiq, M. Mahroof-Tahir, Z.T. Maqsood, K.M. Khan, M.A. Lodhi, M.I. Choudhary, Chemistry, urease inhibition, and phytotoxic studies of binuclear vanadium(IV) complexes, Chem. Biodivers. 4 (2007) 58–71.
[11] P. Hou, Z.-L. You, L. Zhang, X.-L. Ma, L.-L. Ni, Synthesis, characterization, and DNA-binding properties of copper(II), cobalt(II), and nickel(II) complexes with salicylaldehyde 2-phenylquinoline-4-carboylhydrazone, Trans. Met. Chem. 33 (2008) 267–273.
[12] K. Cheng, Q.-Z. Zheng, H.-L. Zhu, Syntheses, structures and urease inhibitory activities of mononuclear cobalt(III) and 1D cobalt(II) complexes with ligands derived from 3-formylsalicylic acid, Inorg. Chem. Commun. 12 (2009) 1116–1119.
[13] K. Cheng, Z.-L. You, H.-L. Zhu, New method for the synthesis of a mononucleating cyclic peptide ligand, crystal structures of its Ni, Zn, Cu, and Co complexes, and their Inhibitory bioactivity against urease, Aust. J. Chem. 60 (2007) 375–379.
[14] Z.-L. You, L.-L. Ni, D.-H. Shi, S. Bai, Synthesis, structures, and urease inhibitory activities of three copper(II) and zinc(II) complexes with 2-{[2-(2-hydroxyethylamino)ethylimino]methyl}-4-nitrophenol, Eur. J. Med. Chem. 45 (2010) 3196–3199.
[15] F. Musiani, E. Arnofi, R. Casadio, S. Ciurli, Structure-based computational study of the catalytic and inhibition mechanisms of urease, J. Biol. Inorg. Chem. 6 (3) (2001) 300–314.
[16] M. Ikram, S.-U. Rehman, S. Rehman, R.J. Baker, C. Schulzke, Synthesis, characterization and distinct butyrylcholinesterase activities of transition metal [Co(II), Ni(II), Cu(II) and Zn(II)] complexes of 2-[(E)-(quinolin-3-ylimino)methyl]phenol, Inorg. Chim. Acta 390 (2012) 210–216.
[17] U. Casellato, P.A. Vigato, Transition metal complexes with binucleating ligands, Coord. Chem. Rev. 23 (1977) 31–117.
[18] K.S. Murray, A.M. Van den Bergen, B.O. West, Ruthenium complexes with a tetradentate salicylaldimine Schiff base, Aust. J. Chem. 58 (1978) 203–207.
[19] H. Doine, Francis F. Stephens, Roderick D. Cannon, Redox behavior of N,N′-ethylenebis(salicylideneaminato)bis(triphenylphosphine)ruthenium(II), Bull. Chem. Soc. Jpn. 58 (1985) 1327–1328.
[20] K. Nakajima, Y. Ando, H. Mano, M. Kojima, Photosubstitution reactivity, crystal structures, and electrochemistry of ruthenium(II)(III) complexes containing tetradentate (O_2N_2, S_2N_2, and P_2N_2) Schiff base ligands, Inorg. Chim. Acta 274 (1998) 184–191.
[21] B. De Clercq, F. Verpoort, Atom transfer radical polymerization of vinyl monomers mediated by Schiff base ruthenium-alkylidene catalysts and the adventitious effect of water in polymerizations with the analogous cationic complexes, Macromolecules 35 (2002) 8943–8947.
[22] T. Opstal, F. Verpoort, Synthesis of highly active ruthenium indenylidene complexes for atom-transfer radical polymerization and ring-opening-metathesis polymerization, Angew. Chem. Int. Ed. 42 (2003) 2876–2879.
[23] T. Opstal, F. Verpoort, Ruthenium indeny-lidene and vinylidene complexes bearing Schiff bases: potential catalysts in Enol–Ester synthesis, Synlett 6 (2002) 935–941.
[24] S.N. Pal, S. Pal, A diruthenum(III) complex possessing a diazine and two chloride bridges: synthesis, structure and properties, Inorg. Chem. 40 (2001) 4807–4810.
[25] B. De Clercq, F. Verpoort, Assessing the scope of the introduction of Schiff bases as co-ligands for monometallic and homobimetallic ruthenium ring-opening metathesis polymerisation and ring-closing metathesis initiators, Adv. Synth. Catal. 34 (2002) 639–648.
[26] B. De Clercq, F. Lefebvre, F. Verpoort, Immobilization of multifunctional Schiff base containing ruthenium complexes on MCM-41, Appl. Catal. A 247 (2003) 345–364.
[27] M.W. Weatherburn, Phenol-hypochloríte reaction for determination of ammonia, Anal. Chem. 39 (1967) 971–974.
[28] I. Khan, S. Ali, S. Hameed, N.H. Rama, M.T. Hussain, A. Wadood, Synthesis, antioxidant activities and urease inhibition of some new 1,2,4-triazole and 1,3,4-thiadiazole derivatives, Eur. J. Med. Chem. 45 (2010) 5200–5207.
[29] R.J.P. Cannell, S.J. Kellam, A.M. Owsianka, J.M. Walker, Results of a large scale screen of microalgae for the production of Protease inhibitors, Planta Med. 54 (1988) 10–14.
[30] M. Ikram, S. Rehman, Faridoon, R.J. Baker, H.U. Rehman, A. Khan, M.I. Choudhary, S.-U. Rehman, Synthesis and distinct urease enzyme inhibitory activities of metal complexes of Schiff-base ligands: kinetic and thermodynamic parameters evaluation from TG–DTA analysis, Thermochim. Acta 555 (2013) 72–80.
[31] O.V. Dolomanov, L.J. Bourhis, R.J. Gildea, J.A.K. Howard, H. Puschmann, OLEX2: a complete structure solution, refinement and analysis program, J. Appl. Cryst. 42 (2009) 339–341.
[32] G.M. Sheldrick, A short history of SHELX, Acta Crystallogr. A 64 (2008) 112–122.
[33] I.-W. Shim, D.-Y. Kim, S. Choi, K.-H. Kong, J.-I. Choe, Reaction chemistry of palladium acetate complexes in polycarbonate: a comparative study, React. Funct. Polym. 43 (3) (2000) 287–296.
[34] H.H. Horowitz, G. Metzger, A new analysis of thermogravimetric traces, Anal. Chem. 35 (10) (1963) 1464–1468.
[35] M. Olszak-Humienik, J. Mozejko, Thermodynamic functions of activated complexes created in thermal decomposition processes of sulphates, Thermochim. Acta 344 (2000) 73–79.
[36] H. Ünver, Z. Hayvalı, Synthesis, spectroscopic studies and structures of square-planar nickel(II) and copper(II) complexes derived from 2-{(Z)-[furan-2-ylmethyl]imino]methyl}-6-methoxyphenol, Spectrochim. Acta Part A: Mol. Biomol. Spectrosc. 75 (2010) 782–786.
[37] Y. Miura, Y. Aritake, T. Akitsu, A chiral photochromic Schiff base: (R)-4-methoxy-2-[(1-phenylethyl)iminomethyl]phenol, Acta Cryst. E 65 (2009) o2381.